The current issue and full text archive of this journal is available at
www.emeraldinsight.com/0961-5539.htm

Application of an ADI scheme for steady and periodic solutions in a lid-driven cavity problem

Manab Kumar Das
Department of Mechanical Engineering, Indian Institute of Technology Guwahati, Guwahati, India, and
P. Rajesh Kanna
Department of Mechanical Engineering, National Taiwan University of Science and Technology, Taipei, Taiwan

Received 31 August 2006
Revised 15 March 2007
Accepted 15 March 2007

Abstract

Purpose – The purpose of the paper is to study the steady and periodic solution of a lid-driven cavity flow problem with the gradual increase of Reynolds number (*Re*) up to 10,000.

Design/methodology/approach – The problem is solved by unsteady stream function-vorticity formulation using the clustered grids. The alternating direction implicit (ADI) method and the central difference scheme have been used for discretization of the governing equations. Total vorticity error and the total kinetic energy have been considered for ensuring the state of flow condition. The midplane velocity distribution and the top wall vortex distribution are compared with the results of other authors and found to show good agreement.

Findings – Kinetic energy variation with time is studied for large time computation. Below 7,500, it becomes constant signifying the flow to be in steady-state. At $Re = 10{,}000$, the fluid flow has an oscillating nature. The dimensionless period of oscillation is found to be 1.63. It is demonstrated that the present computation is able to capture the periodic solution after the bifurcation very accurately.

Originality/value – The findings will be useful in conducting a steady and periodic solution of variety of fluid flows or thermally-driven fluid flows.

Keywords Dynamics, Cavitation, Numerical analysis

Paper type Research paper

Nomenclature

i = x-direction grid point
j = y-direction grid point
L = cavity width
Re = Reynolds number (Re) for the fluid
$\bar{t}$ = dimensional time (s)
t = non-dimensional time
$\bar{u}, \bar{v}$ = dimensional velocity components along (x, y) axes (m/s)
u, v = dimensionless velocity components along (x, y) axes
$\bar{U}$ = lid velocity (m/s)
$\bar{x}, \bar{y}$ = dimensional Cartesian co-ordinates along and normal to the plate (m)
x, y = dimensionless Cartesian co-ordinates along and normal to the plate

Greek symbols

ε = convergence criterion
κ = clustering parameter
ψ = dimensionless stream function
ω = dimensionless vorticity

Subscripts

c = critical
w = wall

International Journal of Numerical Methods for Heat & Fluid Flow
Vol. 17 No. 8, 2007
pp. 799-822

0961-5539
DOI 10.1108/09615530710825783

1. Introduction

Lid driven cavity problem is extensively studied because of its certain flow features. Boundary layer on the wall, flow separation from one wall and reattachment on the perpendicular wall, attachment and separation from the same wall, multiple separation and attachment, vortices, bubbles are some interesting features of this problem (Figure 1(a)). Almost all numerical methods for fluid flow developed are tested with this problem for accuracy. Probably the first systematic numerical study of square lid driven cavity flow problem was given by Burggraf (1966). Using a stream function-vorticity formulation, he was able to predict up to *Re* (*Re*) $= 400$ and compared the result with Batchelor's model. Nallasamy and Prasad (1977) investigated the problem for $Re = 0$-50,000. They have used unsteady stream function-vorticity formulation and ADI (alternating direction implicit) with higher order upwinding scheme. However, their results are limited by the choice of less number of grids which gave an under-resolved solution. In spite of that, they were able to predict qualitatively the appearance and relative size of the primary and secondary vortices. Benjamin and Denny (1979) used a transformed equation to implement non-uniform grids in the domain. They have solved in unsteady stream function-vorticity formulation for *Re* up to 10,000. Their prediction about vortices are very good but the velocity distribution were not given for comparisons. It seems that they were able to understand a periodic transition of flow when *Re* is increased beyond 10,000. Ghia's *et al.* (1982) work is usually considered as a benchmark solution for validating numerical schemes. In this work, multi-grid streamfunction formulation is used in the transient form of equation.

Schreiber and Keller (1983a), and Kim and Moin (1985) developed new schemes and compared with Ghia's *et al.* (1982) result. Schreiber and Keller (1983b) pointed out about the possible spurious solution. Schreiber and Keller (1983a) also pointed out about the possible transition from laminar to turbulent flow. Gustafson and Halasi (1986), considering unsteady Navier-Stokes equation (NSE) in primitive variable, have solved up to $Re = 5{,}000$. They have raised the question that

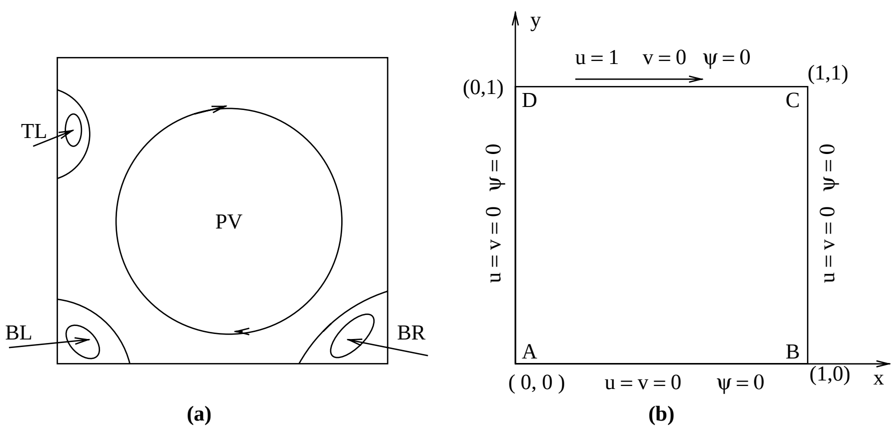

Note: PV-Primary vortex, BL-Bottom left vortex, BR-Bottom right vortex, TL-Top left vortex

Figure 1.
Schematic diagram with boundary condition of lid driven cavity problem

probably the flow undergoes a transition from laminar to turbulent as *Re* is increased above 5,000. This information has led to the further investigation of unsteady-state lid driven cavity problem.

Sohn (1988) has considered the steady-state equation of the problem to validate the commercial software FIDAP. He has solved for *Re* up to 10,000 and compared the results with Ghia *et al.* (1982). His results are close. However, no further information is available. The work of Goodrich *et al.* (1990), though carried out for aspect ratio (AR = ratio of depth to width) two, is relevant in this context. They have described several convergence criteria to ascertain whether an unsteady flow has reached a steady-state after considerable time marching integration steps. Similar criteria have been followed by several researchers and also followed in this paper. Bruneau and Jouron (1990) considering a steady-state formulation in primitive variable NSE, solved the problem up to $Re = 15{,}000$. They observed that there is a loss of convergence as *Re* is increased to 10,000. They have reported that this is probably due to the transition taking place from laminar to turbulent flow. This is important in the context whether $Re = 10{,}000$ solution is steady or unsteady. Shen (1990) has reported that the transition is occuring for *Re* in the range of 10,000-12,000. Later on, Shen (1991) has reported that the critical $Re = Re_c$ lies between 10,000 and 10,500. Huser and Biringen (1992) considered unsteady equation in primitive variable and reported up to $Re = 30{,}000$ for shear driven cavity flow problems. Similar type of unsteadiness is observed as *Re* is increased beyond 11,100. They have used total kinetic energy (TKE) criterion to ensure the attainment of steady state.

Cortes and Miller (1994) studied the lid-driven cavity problem for AR equal to 1 and 2 in primitive variable formulation. They have observed that in case of square cavity, the flow attains an unsteady state for $Re = 10{,}000$. However, detail results are not provided. Hou *et al.* (1995) solved the NSE by lattice Botlzmann method. They have observed a bifurcation between $Re = 7{,}500$ and 10,000. The flow oscillates between a series of different configurations. That is why they have presented results for *Re* up to 7,500. Poliashenko and Aidun (1995) have given a direct method of bifurcation problem. They have computed the sequence of transitions from steady to chaotic flow in the lid-driven cavity problem.

Liao and Zhu (1991) have solved the steady state equations in the stream function-vorticity formulation. They have reported steady state solution up to $Re = 10{,}000$. Goyon (1996) has considered the unsteady equation and solved for high $Re = 10{,}000$. He has reported that steady state solution is observed by considering the convergence criteria for streamfunction and vorticity. However, unsteady solution is obtained by considering the TKE as the convergence criterion. The critical *Re* observed by him is between 10,000 and 12,500.

In an extensive study of Barragy and Carey (1997), stable steady results are reported for *Re* up to 12,500. A detailed result about the various vortices and velocity distribution are reported to be used as the benchmark solutions. Absence of transition in this study raises a serious question about the transition of flow with increase in *Re*. In a recent study, Peng and Shiau (1991) observed several branches of bifurcation. The unsteadiness started with $Re = 7{,}402 \pm 4$ percent which is followed by several branches at different *Re*. They studied up to $Re = 11{,}000$.

Erturk *et al.* (2005) have presented a steady solutions for $Re < 21{,}000$. The Navier-Stokes equation in stream function-vorticity formulation are solved numerically using a fine uniform mesh of 601 × 601. They concluded that fine mesh is required in order to obtain a steady solution.

Recently, Bruneau and Saad (2006) have reported the accurate results for steady and periodic solutions around the critical *Re*. They have solved the equations in primitive variable form with higher-order upwinding schemes. They have studied the linear stability problem by computing the first Lyapunov exponent of the linearized system. They concluded that the critical *Re* is $8{,}000 < Re_c < 8{,}050$ within 1 percent of error. They have also reported the periodic solution at $Re = 10{,}000$ for grid 512 × 512 and 1,024 × 1,024 and reported a frequency of $f = 0.61$. A summary of the discussion made above is given in Table I.

From this literature survey it is observed that the phenomena of transition from steady- to unsteady-state solution has been noticed recently and which is yet to be established. However, one conclusion can be drawn that up to $Re = 7{,}500$, the flow remains steady and all the results in literature should match and be taken as benchmark solutions. Solution above $Re = 7{,}500$ should be studied thoroughly and be considered cautiously for benchmarking.

In this present study, an unsteady stream function-vorticity equation has been solved by ADI method. All the terms have been discretized by central difference scheme so that the results are free of artificial diffusion. Steady-state is reached asymptotically with time marching. Two criteria for steady-state condition have been used viz. the total vorticity error and the TKE. *Re* is varied to 100, 400, 1,000, 3,200, 5,000, 7,500 and 10,000 (Ghia *et al.*, 1982). Steady-state is obtained up to $Re = 7{,}500$. For $Re = 10{,}000$, the TKE showed oscillations implying an unsteady-state. It will be shown that even with less number of grids, the present formulation is able to capture the periodicity of oscillation for $Re = 10{,}000$.

2. Mathematical formulation

The governing equations for incompressible laminar flow are solved by stream function-vorticity formulation. The transient non-dimensional governing equations in the conservative form are, stream function equation:

$$\nabla^2 \psi = -\omega \qquad (1)$$

Vorticity equation:

$$\frac{\partial \omega}{\partial t} + \frac{\partial (u\omega)}{\partial x} + \frac{\partial (v\omega)}{\partial y} = \frac{1}{Re}\nabla^2 \omega \qquad (2)$$

where ψ – stream function, $u = \partial\psi/\partial y$; $v = -\partial\psi/\partial x$ and $\omega = (\partial v/\partial x) - (\partial u/\partial y)$.

The variables are scaled as:

$$u = \frac{\bar{u}}{\bar{U}}; v = \frac{\bar{v}}{\bar{U}}; x = \frac{\bar{x}}{L}; y = \frac{\bar{y}}{L}; \omega = \frac{\bar{\omega}}{\bar{U}/L}; t = \frac{\bar{t}}{L/U}$$

with the overbar indicating a dimensional variable and $\bar{U}$, L denoting the lid velocity and the length of the cavity, respectively.

The boundary conditions needed for the numerical simulation have been prescribed. The schematic diagram along with the boundary conditions is shown in Figure 1(b).

Table I. Literature survey

Author	Formulation	Steady/unsteady equation	Range of reconsidered	Remarks on transition
Nallasamy and Prasad (1977)	Streamfunction and vorticity	Unsteady	0-50,000	Not reported
Benjamin and Denny (1979)	Streamfunction and vorticity	Unsteady	0-10,000	Hinted transition
Ghia *et al.* (1982)	Streamfunction and vorticity	Unsteady	0-10,000	Not reported
Schreiber and Keller (1983a)	Streamfunction and vorticity	Steady	0-10,000	Hinted about transition
Kim and Moin (1985)	Primitive variable	Unsteady	0-5,000	Not reported
Gustafson and Halasi (1986)	Primitive variable	Unsteady	0-5,000	First to point out about transition
Sohn (1988)	Primitive variable	Steady	0-10,000	Not reported
Goodrich *et al.* (1990)	Primitive variable	Unsteady	0-12,500	Delineated criteria for attaining steady state
Bruneau and Jouron (1990)	Primitive variable	Steady	0-15,000	For $Re_c > 5,000$, reported loss of stability
Shen (1990)	Primitive variable	Unsteady	0-12,000	Re_c in the range of 10,000-12,000
Shen (1991)	Primitive variable	Unsteady	0-12,500	Re_c in the range of 10,000-10,500
Huser and Biringen (1992)	Primitive variable	Unsteady	30,000	Reported about occurrence of transition
Liao and Zhu (1991)	Streamfunction and vorticity	Steady	10,000	Reported stable solution
Cortes and Miller (1994)	Primitive variable	Unsteady	0-10,000	Reported about unstable solution
Hou *et al.* (1995)	Lattice Boltzmann method		7,500	Re_c above 7,500
Poliashenko and Aidun (1995)	Direct method	Unsteady	–	$Re_c = 7,763 \pm 2$ percent
Goyon (1996)	Streamfunction and vorticity	Unsteady	0-12,500	$10,000 < Re_c < 12,500$
Barragy and Carey (1997)	Streamfunction and vorticity	Steady	0-12,500	Stable
Peng and Shiau (1991)	Primitive variable	Unsteady	11,000	$Re_c = 7,402 \pm 4$ percent
Erturk *et al.* (2005)	Streamfunction and vorticity	Pseudo time derivative	21,000	Steady
Bruneau and Saad (2006)	Primitive variable	Unsteady	10,000	$8,000 < Re_c < 8,050$

Along AB, BC and AD, due to no-slip condition:

$$u = v = 0 \tag{3a}$$

Along CD:

$$u = 1, v = 0. \tag{3b}$$

3. Numerical procedure

The unsteady vorticity transport equation (2) in time is solved by alternate direction implicit scheme (ADI). The central differencing scheme is followed for both the convective as well as the diffusive terms (Roache, 1998; Briley, 1971). It consists of two half time-steps.

The first half time-step:

$$\begin{gathered}\frac{\omega_{i,j}^{n+(1/2)} - \omega_{i,j}^{n}}{\Delta t/2} + Lx(u\omega)_{i,j}^{n+(1/2)} + Ly(v\omega)_{i,j}^{n} \\ - \frac{1}{Re}\left(Lxx(\omega)_{i,j}^{n+(1/2)} + Lyy(\omega)_{i,j}^{n}\right) = 0.\end{gathered} \tag{4a}$$

The second half time-step:

$$\begin{gathered}\frac{\omega_{i,j}^{n+1} - \omega_{i,j}^{n+(1/2)}}{\Delta t/2} + Lx(u\omega)_{i,j}^{n+(1/2)} + Ly(v\omega)_{i,j}^{n+1} \\ - \frac{1}{Re}\left(Lxx(\omega)_{i,j}^{n+(1/2)} + Lyy(\omega)_{i,j}^{n+1}\right) = 0\end{gathered} \tag{4b}$$

where:

$$\begin{aligned}Lx(u\omega)_{i,j} &= \frac{(u\omega)_{i+1,j} - (u\omega)_{i-1,j}}{\Delta x_i + \Delta x_{i-1}}, \\ Ly(v\omega)_{i,j} &= \frac{(v\omega)_{i,j+1} - (v\omega)_{i,j-1}}{\Delta y_j + \Delta y_{j-1}}\end{aligned} \tag{5a}$$

$$\begin{aligned}Lxx(\omega)_{i,j} &= \frac{\omega_{i-1,j} - 2\omega_{i,j} + \omega_{i+1,j}}{\Delta x_i * \Delta x_i - 1}, \\ Lyy(\omega)_{i,j} &= \frac{\omega_{i,j-1} - 2\omega_{i,j} + \omega_{i,j+1}}{\Delta y_j * \Delta y_{j-1}}.\end{aligned} \tag{5b}$$

Equations (4a) and (4b) are rearranged to give the following equations (6a) and (6b).

$$\begin{gathered}-\left(C_x u_{i-1,j}^{n} + S_x\right)\omega_{i-1,j}^{n+(1/2)} + (1 + 2S_x)\omega_{i,j}^{n+(1/2)} - \left(-C_x u_{i+1,j}^{n} + S_x\right)\omega_{i+1,j}^{n+(1/2)} \\ = \left(C_y v_{i,j-1}^{n} + S_y\right)\omega_{i,j-1}^{n} + (1 - 2S_y)\omega_{i,j}^{n} + \left(-C_y v_{i,j+1}^{n} + S_y\right)\omega_{i,j+1}^{n}\end{gathered} \tag{6a}$$

$$-\left(C_y v^n_{i-1,j} + S_y\right)\omega^{n+1}_{i,j-1} + (1+2S_y)\omega^{n+1}_{i,j} - \left(-C_y v^n_{i,j+1} + S_y\right)\omega^{n+1}_{i,j+1}$$

$$= \left(C_x u^n_{i-1,j} + S_x\right)\omega^{n+(1/2)}_{i-1,j} + (1-2S_x)\omega^{n+(1/2)}_{i,j} + \left(-C_x u^n_{i+1,j} + S_x\right)\omega^{n+(1/2)}_{i+1,j} \quad (6b)$$

where:

$$C_x = \frac{\Delta t}{2(\Delta x_i + \Delta x_{i-1})},$$

$$C_y = \frac{\Delta t}{2(\Delta y_i + \Delta y_{j-1})},$$

$$S_x = \frac{\Delta t}{Re}\ \frac{1}{\Delta x_i * (\Delta x_i + \Delta x_{i-1})},$$

$$S_y = \frac{\Delta t}{Re}\ \frac{1}{\Delta y_j * (\Delta y_j + \Delta y_{j-1})}.$$

The discretization of equation (1) is given by:

$$Lxx(\psi) + Lyy(\psi) = -\omega_{i,j}. \quad (7)$$

The velocity components are updated by the following equations:

$$u = \frac{\partial \psi}{\partial y} = \frac{\psi_{i,j+1} - \psi_{i,j-1}}{\Delta y_i + \Delta y_{j-1}} \quad (8a)$$

$$v = -\frac{\partial \psi}{\partial x} = -\frac{\psi_{i+1,j} - \psi_{i-1,j}}{\Delta x_i + \Delta x_{i-1}}. \quad (8b)$$

The velocities (equations (6a) and (6b)) are calculated at nth time level while advancing to the $(n+1)$th time level. Because of this approximation in the non-linear terms, the second order accuracy of the method is somewhat lost. However, something of the second-order accuracy of the linearized system is retained if the velocity field is slowly varying (Roache, 1998).

It is first order accurate in time and second order accurate in space $O(\Delta t, \Delta x^2, \Delta y^2)$, and is unconditionally stable. The Poisson equation (7) is solved explicitly by five point Gauss-Seidel methods. Thom's vorticity condition has been used to obtain the wall vorticity as given below:

$$\omega_\omega = -\frac{2(\psi_{\omega+1} - \psi_\omega)}{\Delta n^2} \quad (9)$$

where Δn is the grid space normal to the wall. It has been shown by Napolitano *et al.* (1999) and Huang and Wetton (1996) that convergence in the boundary vorticity is actually second order for steady problems and for time-dependent problems when $t > 0$. Roache (1998) has reported that for a Blausius boundary-layer profile, numerical test verify that this first-order form is more accurate than second-order form.

Solution approaches steady-state asymptotically while the time reaches infinity. The computational domain considered here is clustered Cartesian grids. For unit length, the grid space at ith node is (Kuyper *et al.*, 1993):

$$x_i = \left(\frac{i}{i_{\max}} - \frac{k}{\upsilon} \sin\left(\frac{i\upsilon}{i_{\max}} \right) \right) \tag{10}$$

where υ is the angle and κ is the clustering parameter. $\upsilon = 2\pi$ stretches both end of the domain whereas $\upsilon = \pi$ clusters more grid points near one end of the domain. κ varies between 0 and 1. When it approaches 1, more points fall near the end.

The convergence criteria are to be set in such a way that it should not terminate at a false stage. At steady-state, the error reaches the asymptotic behavior. Here, it is set as sum of vorticity error reduced to either the convergence criteria ε (equation (11)) or a large total time:

$$\sum_{i,j=1}^{i_{\max}\ j_{\max}} \left| \left(\omega_{i,j}^{t+\Delta t} - \omega_{i,j}^{t} \right) \right| < \varepsilon. \tag{11}$$

4. Results and discussion

The lid-driven square cavity flow problem has been computed for $1 \leq Re \leq 10{,}000$. Comparison has been done with Ghia *et al.* (1982), Barragy and Carey (1997), Rek and Skerget (1994) and Schreiber and Keller (1983a). This paper consists of three parts such as:

(1) the validation of the present computations;

(2) study of the periodic solution; and

(3) proposed new results to be used as a benchmark solution.

4.1 Validation

The minimum time step used is 0.001 for $Re = 10{,}000$, $0 < t < 360$ by Goodrich *et al.* (1990). In the present computations, time step 0.001 is used for $100 < Re < 3{,}200$ and 0.01 for $Re > 3{,}200$. However, for $Re = 1{,}100$ time step 0.0001 is used. Low *Re* results are used as initial value for high *Re* computation (Comini *et al.*, 1994). As pointed out by Goyon (1996), the thinning of the wall boundary layers is very low for $Re > 3{,}200$. Because of this reason, the grid independence study is carried out for two *Re*, viz. $Re = 3{,}200$ and 10,000 (Figure 2). For $Re < 3{,}200$, a grid system of 101×101 is used. For $Re > 3{,}200$, the 129×129 grid system is used. From the clustering function the minimum grid size occurred near the wall is $\Delta x = 0.002346$, $\Delta y = 0.002346$ for the grid system 101×101 and $\Delta x = 0.002346$, $\Delta y = 0.002346$ for the grid system 129×129. It is of interest to note that these grids are smaller than the uniform grid size 1/257 used by Ghia *et al.* (1982).

The minimum stream function value at primary vortex is listed at Tables II and III. It is noticed that the stream function value is increased up to $Re = 5{,}000$ and further it is decreased. Similar variations are presented in Ghia *et al.* (1982) and Rek and Skerget (1994). However, its value has an increasing trend for (Barragy and Carey, 1997). This clearly shows the good agreement of the strength of the stream function with the benchmark results. Primary vortex value and its corresponding *x*-coordinate location as well as *y*-coordinate location are tabulated in details at Tables IV-VI. *Tecplot 9.0-0.9* (2001) is used to extract these values from stream function contours. It is noticed that for $Re < 100$, the center of the primary vortex moves from the horizontal middle location to positive *x* direction.

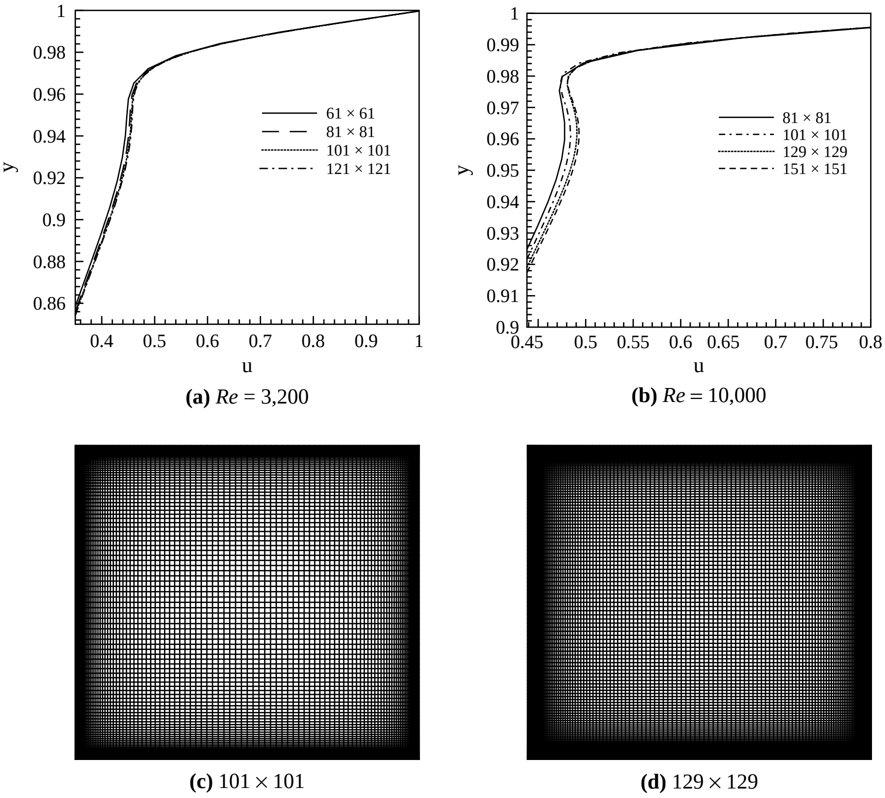

Figure 2.
Grid independence study

Re	ψ	ψ^a	ψ^b	ψ^c
1	−0.099919	−0.10005	–	−0.10006
100	−0.103394	−0.10330	−0.103423	−0.10330
400	−0.113801	−0.11389	−0.113909	−0.11297
1,000	−0.118496	−0.11861	−0.117929	−0.11603

Source: [a]Barragy and Carey (1997), [b]Ghia *et al.* (1982) and [c]Schreiber and Keller (1983a)

Table II.
Primary vortex streamfunction value

Re	ψ	ψ^a	ψ^b	F^c
3,200	−0.120762	–	−0.120377	–
5,000	−0.121195	−0.1222194	−0.118966	–
7,500	−0.120882	−0.1223803	−0.119976	–
10,000	−0.117948	−0.122393	−0.119731	−0.10284

Source: [a]Barragy and Carey (1997), [b]Ghia *et al.* (1982) and [c]Schreiber and Keller (1983a)

Table III.
Primary vortex streamfunction value

Further, it moves back to the center of the geometry. When *Re* increases from 1, the viscous layer thickness adjacent to moving wall is increased in the downstream direction. This is attributed to the movement of vortex center in the positive *x* direction. With further increase in *Re*, the viscous layer thickness from the right wall is also increased. Owing to this, the vortex center moves towards the center of the geometry. The bottom right corner vortices, left wall vortices and upper left corner vortices are shown in Tables VII-XI. The comparisons show good agreement for these vortices. However, the tertiary vortex at lower left corner is not captured in this computations.

The $u-$ velocity along the vertical line passing through the geometric center is compared with Rek and Skerget (1994) and Ghia *et al.* (1982) (Figure 3). It showed a good agreement with the results of other authors. The $v-$ velocity along horizontal line passing through geometric center is compared with Ghia *et al.* (1982). The results show

Table IV. Primary vortex stream function location

Re	ψ (x_{loc}, y_{loc})	ψ^{a} (x_{loc}, y_{loc})
1	−0.099919 (0.500139, 0.763206)	−0.10006 (0.5000, 0.76667)
20	−0.099958 (0.532567, 0.774311)	–
40	−0.100490 (0.557842, 0.754127)	−0.10060 (0.56667, 0.75833)
60	−0.100934 (0.574561, 0.752207)	–
80	−0.102160 (0.590142, 0.745027)	–

Source: [a]Schreiber and Keller (1983a)

Table V. Primary vortex streamfunction location

Re	ψ (x_{log}, y_{loc})	ψ^{a} (x_{loc}, y_{loc})	ψ^{b} (x_{loc}, y_{loc})	ψ^{c} (x_{loc}, y_{loc})
100	−0.103394	−0.10330	−0.103423	−0.10330
–	(0.617562, 0.740202)	–	(0.6172, 0.7344)	(0.61667, 0.74167)
400	−0.113801	−0.11389	−0.113909	−0.11297
–	(0.55101, 0.601142)	–	(0.5547, 0.6055)	(0.55714, 0.60714)
1,000	−0.118496	−0.11861	−0.117929	−0.11603
–	(0.53410, 0.567841)	–	(0.5313, 0.5625)	(0.52857, 0.56429)

Source: [a]Barragy and Carey (1997); [b]Ghia *et al.* (1982) and [c]Schreiber and Keller (1983a)

Table VI. Primary vortex streamfunction location

Re	ψ (x_{loc}, y_{loc})	ψ^{a} (x_{loc}, y_{loc})	ψ^{b} (x_{loc}, y_{loc})	ψ^{c} (x_{loc}, y_{loc})
3,200	−0.120762	–	−0.120377	–
	(0.517132, 0.534112)	–	(0.5165, 0.5469)	–
5,000	−0.121195	−0.1222194	−0.118966	–
	(0.51542, 0.539923)	(0.5151064, 0.5358696)	(0.5117, 0.5352)	–
7,500	−0.120882	−0.1223803	−0.119976	–
	(0.51342, 0.526685)	(0.5132184, 0.5320950)	(0.5117, 0.5322)	–
10,000	−0.117948	−0.122393	−0.119731	−0.10284
	(0.513419, 0.526702)	(0.5113304, 0.53202077)	(0.5117, 0.5333)	(0.51397, 0.53073)

Source: [a]Barragy and Carey (1997); [b]Ghia *et al.* (1982) and [c]Schreiber and Keller (1983a)

Re	ψ (x_{loc}, y_{loc})	ψ^a (x_{loc}, y_{loc})	ψ^b (x_{loc}, y_{loc})
1	2.999998×10^{-6}		2.4700×10^{-6}
	(0.965253, 0.034519)	–	(0.96667, 0.03333)
100	1.3×10^{5}	1.25374×10^{-5}	1.320×10^{-5}
	(0.939954, 0.059880)	(0.9453, 0.0625)	(0.94167, 0.05000)
400	6.483×10^{-4}	6.42352×10^{-4}	6.440×10^{-4}
	(0.88555, 0.122909)	(0.8906, 0.1250)	(0.88571, 0.11429)
1,000	1.7549×10^{-3}	1.75102×10^{-3}	1.700×10^{-3}
	(0.871406, 0.11105)	(0.8594, 0.1094)	(0.86429, 0.10714)

Source: [a]Ghia *et al.* (1982) and [b]Schreiber and Keller (1983a)

Table VII. Vortices in lower right corner

Re	ψ (x_{loc}, y_{loc})	ψ^a (x_{loc}, y_{loc})	ψ^b (x_{loc}, y_{loc})	ψ^c (x_{loc}, y_{loc})
3,200	0.002912		0.00313955	
	(0.829335, 0.079221)	–	(0.8125, 0.0859)	–
5,000	3.1230×10^{-3}	3.073515×10^{-3}	3.08358×10^{-3}	
	(0.80172, 0.072269)	(0.804102, 0.0724865)	(0.8086, 0.0742)	
	-1.8756×10^{-6}	-1.42791×10^{-6}	-1.43226×10^{-6}	
	(0.97784, 0.019192)	(0.978601, 0.01881959)	(0.9805, 0.0195)	–
7,500	3.30297×10^{-3}	3.22698×10^{-3}	3.28484×10^{-3}	
	(0.790459, 0.0636501)	(0.790025, 0.0064834)	(0.7813, 0.0625)	
	-3.08765×10^{-5}	-3.27901×10^{-5}	-3.28148×10^{-5}	
	(0.95217, 0.0396103)	(0.95174, 0.042289)	(0.9492, 0.0430)	–
10,000	3.4601×10^{-3}	3.1912×10^{-3}	3.41831×10^{-3}	2.960×10^{-3}
	(0.780553, 0.0634046)	(0.7746636, 0.0587801)	(0.7656, 0.0586)	(0.78771, 0.06145
	-1.20×10^{-4}	-1.40446×10^{-4}	-1.31321×10^{-4}	
	(0.940851, 0.063843)	(0.935165, 0.0675283)	(0.9336, 0.0625)	

Source: [a]Barragy and Carey (1997); [b]Ghia *et al.* (1982) and [c]Schreiber and Keller (1983a)

Table VIII. Vortices in lower right corner

Re	ψ (x_{loc}, y_{loc})	ψ^a (x_{loc}, y_{loc})	ψ^b (x_{loc}, y_{loc})
1	2.99997×10^{-6}		2.440×10^{-6}
	(0.0345193, 0.0345188)	–	(0.03333, 0.0333)
100	2.0×10^{-6}	1.74877×10^{-6}	2.050×10^{-6}
	(0.034504, 0.0345977)	(0.0313, 0.0391)	(0.03333, 0.025)
400	1.5×10^{-5}	1.41951×10^{-5}	1.450×10^{-5}
	(0.048793, 0.048794)	(0.0508, 0.0469)	(0.0500, 0.04286)
1,000	2.2358×10^{-4}	2.31129×10^{-4}	2.170×10^{-4}
	(0.082206, 0.079223)	(0.0859, 0.0781)	(0.08571, 0.07143)

Source: [a]Ghia *et al.* (1982) and [b]Schreiber and Keller (1983a)

Table IX. Vortices in lower left corner

good agreement (Figure 4). The moving wall vorticity is compared with Ghia *et al.* (1982) and Rek and Skerget (1994). The present results show very good agreement with their results. However, it showed excellent agreement with Ghia *et al.* (Figure 5) even at high *Re*. The vorticity separation points along the left wall, i.e. where the vorticity

Table X. Vortices in lower left corner

Re	ψ (x_{loc}, y_{loc})	ψ^{a} (x_{loc}, y_{loc})	ψ^{b} (x_{loc}, y_{loc})
3,200	1.119×10^{-3} (0.079221, 0.11951)	–	0.97823×10^{-3} (0.0859, 0.1094)
5,000	1.373×10^{-3} (0.073602, 0.138583)	1.3765×10^{-3} (0.0724865, 0.137029)	1.36119×10^{-3} (0.0703, 0.1367)
7,500	1.524×10^{-3} (0.06363, 0.154805)	1.5364×10^{-3} (0.0641618, 0.1525889)	$1.46709 \times 10^{-}$ (0.0645, 0.1504)
10,000	1.898×10^{-3} (0.1029, 0.123542)	1.61957×10^{-3} (0.05878, 0.16229)	1.51829×10^{-3} (0.0586, 0.1641)

Source: [a]Barragy and Carey (1997) and [b]Ghia *et al.* (1982)

Table XI. Vortices in upper left corner

Re	ψ (x_{loc}, y_{loc})	ψ^{a} (x_{loc}, y_{loc})	ψ^{b} (x_{loc}, y_{loc})
3,200	7.250×10^{-4} (0.054167, 0.89781)	–	7.27682×10^{-4} (0.0547, 0.8984)
5,000	1.4540×10^{-3} (0.063625, 0.909455)	1.4476×10^{-3} (0.063488, 0.909248)	1.45641×10^{-3} (0.0625, 0.9102)
7,500	2.120×10^{-3} (0.068519, 0.909465)	2.134407×10^{-3} (0.06688547, 0.911632)	2.04620×10^{-3} (0.0664, 0.9141)
10,000	2.9740×10^{-3} (0.068519,0.909466)	2.6304×10^{-3} (0.070224, 0.910838)	2.42103×10^{-3} (0.0703, 0.9141)

Source: [a]Barragy and Carey (1997) and [b]Ghia *et al.* (1982)

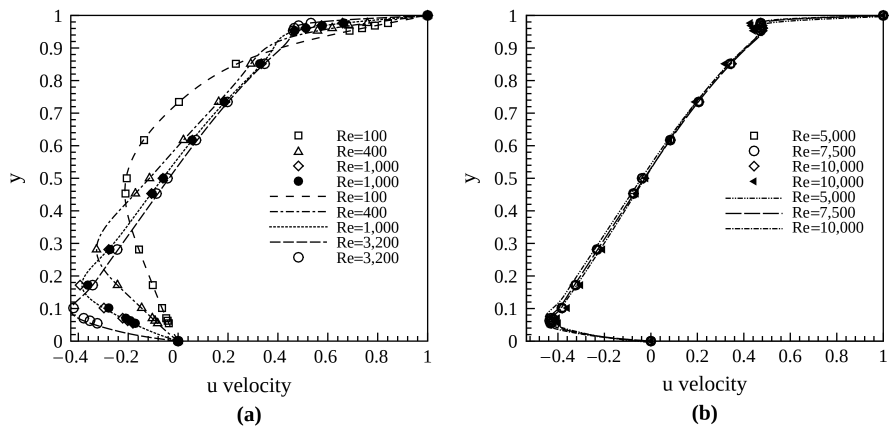

Figure 3. Vertical centerline u – velocity passing through geometric center

Note: Open symbols (Ghia *et al.*, 1982), close symbol (Rek and Skerget, 1994) and line patterns - present results

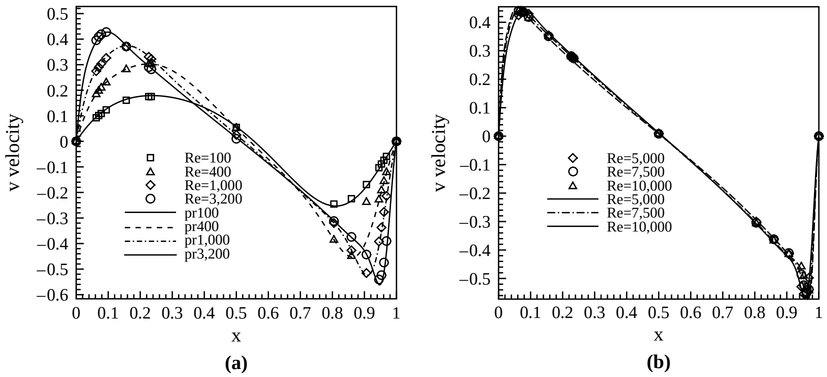

Note: Open symbols (Ghia *et al.*, 1982), close symbol (Rek and Skerget, 1994) and line patterns - present results

Figure 4. Horizontal centerline v – velocity passing through geometric center

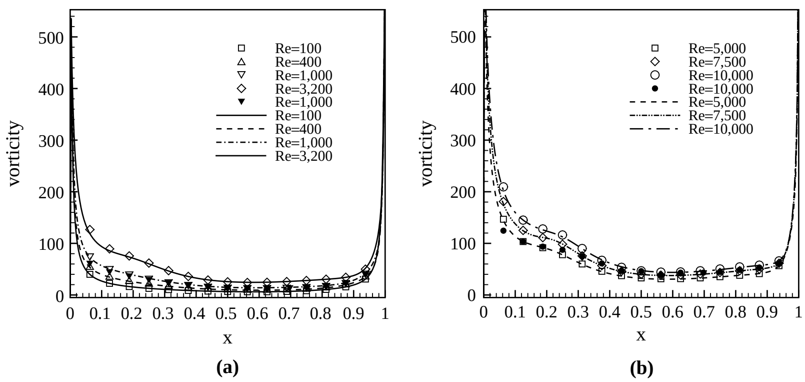

Note: Open symbols (Ghia *et al.*, 1982), close symbol (Rek and Skerget, 1994) and line patterns - present results

Figure 5. Moving wall vorticity

signs are changing, are compared for wide range of Re with Barragy and Carey (1997) (Figure 6). It is having a good agreement with their results. However, the present study has been conducted for maximum $Re = 10{,}000$. For this range it showed good agreement.

The stream line contours for different time level is presented in Figure 7 for $Re = 1{,}000$. Initial time step is used as 10^{-6} up to the time reaches 1, and for further computation, a time step of 10^{-3} is used. There is no vortex formation at $t = 1.4 \times 10^{-4}$ (Figure 7(a)). At time = 1.328 a recirculation is created near the top wall right corner (Figure 7(b)). While time increases this first recirculation is moving towards the center of the geometry Figure 7(c). At time $t = 5.027$ a small secondary recirculation is created at the right bottom of the domain. Simultaneously another recirculation is created at middle of the right wall (Figure 7(d)). This middle recirculation moves in the negative y direction and mixes with the bottom right recirculation (Figure 7(e)). At time $t = 11.836$, another secondary recirculation is

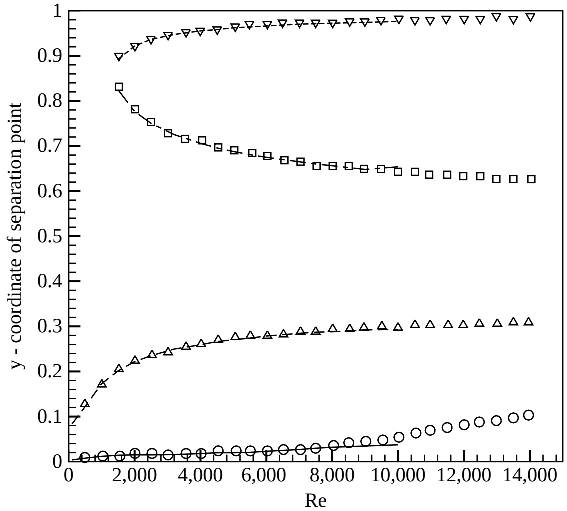

Figure 6.
Left wall separation points

Note: Open symbols (Barragy and Carey, 1997) and line patterns - present results

formed at the bottom left corner 7(f). The time evolution of the mid-plane *u* velocity distribution is shown in Figure 8. It is observed that the effect of the top wall is gradually penetrating towards the bottom wall. When the solution reaches an asymptotic value, the secondary recirculations are positioned stably at both the bottom corners. The stream line contours for wide range of *Re* are shown in Figure 9. With increase of *Re,* the size of the vortices at the bottom corners increases. Also, a tertiary vortex appears in the bottom right corner.

4.2 Study of the periodic solution

The linear stability problem of the first bifurcation has been studied in details by Bruneau and Saad (2006). They have reported the critical *Re* when the steady solution loses its stability to the benefit of a periodic solution, which corresponds to the localization of the first Hopf bifurcation. This was done by computing the first Lyapunov exponent of the linearized system. They have concluded from numerical tests that the critical *Re* for the 2D lid-driven cavity problem is $8{,}000 < Re_c < 8{,}050$ within less than 1 percent accuracy.

The purpose of the present study is to capture the periodic solution at the particular $Re = 10{,}000$ by the present numerical method. For this purpose, the criterion considered is the TKE. The TKE expression (Goyon, 1996) is given by:

$$E(n \times \delta t) = \left(\sum_{(i,j)=(1,1)}^{(nx,ny)} \left[\left(u_{i,j}^n\right)^2 + \left(v_{i,j}^n\right)^2 \right] \right)^{1/2}. \qquad (12)$$

Figure 10 shows the convergence history of the TKE. Figure 10(a) shows the early stage kinetic energy for different *Re*. Kinetic energy gradually increases as time increases. It is noticed that the case $Re = 1{,}000$ has become time independent at

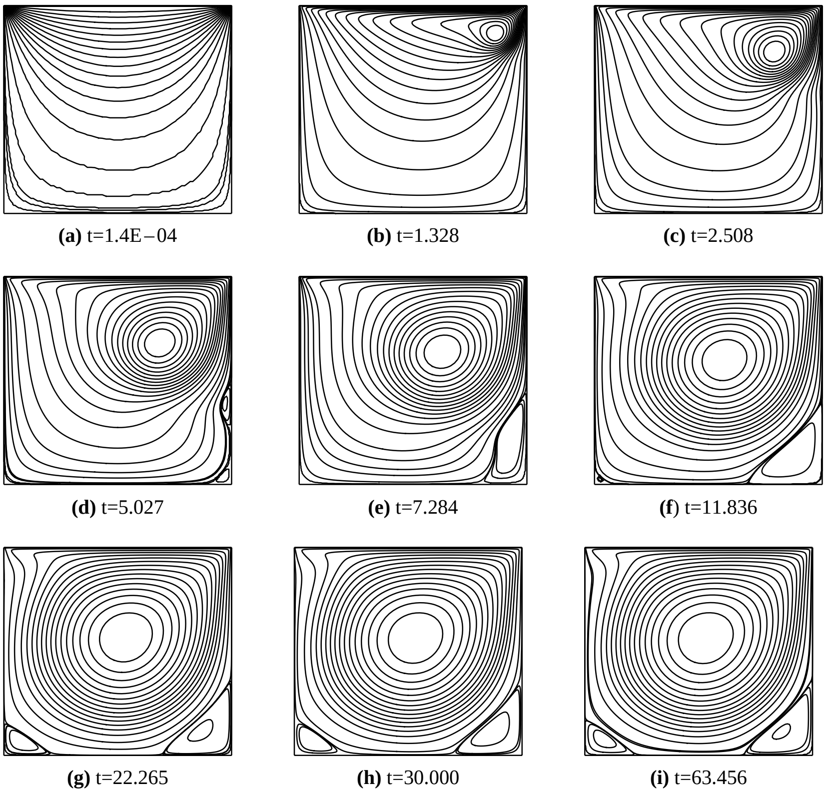

Figure 7.
Transient results: $Re = 1{,}000$, streamline contour

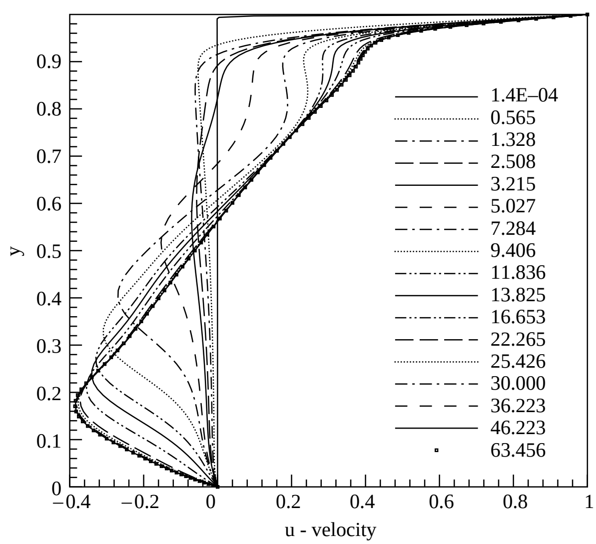

Figure 8.
Transient results: u velocity along the vertical centerline through the geometric center

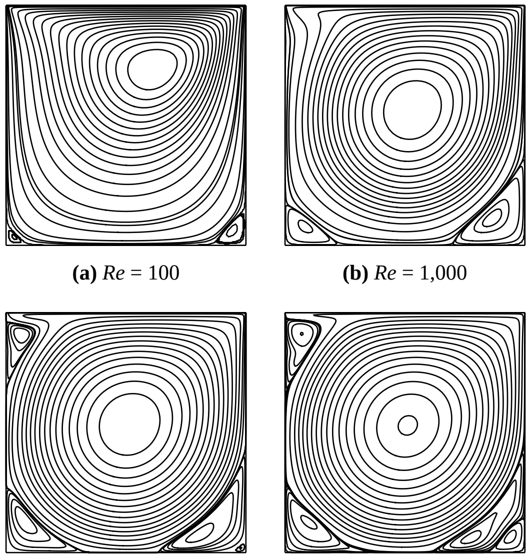

(a) *Re* = 100 (b) *Re* = 1,000 (c) *Re* = 5,000 (d) *Re* = 10,000

Figure 9.
Streamline contour for various

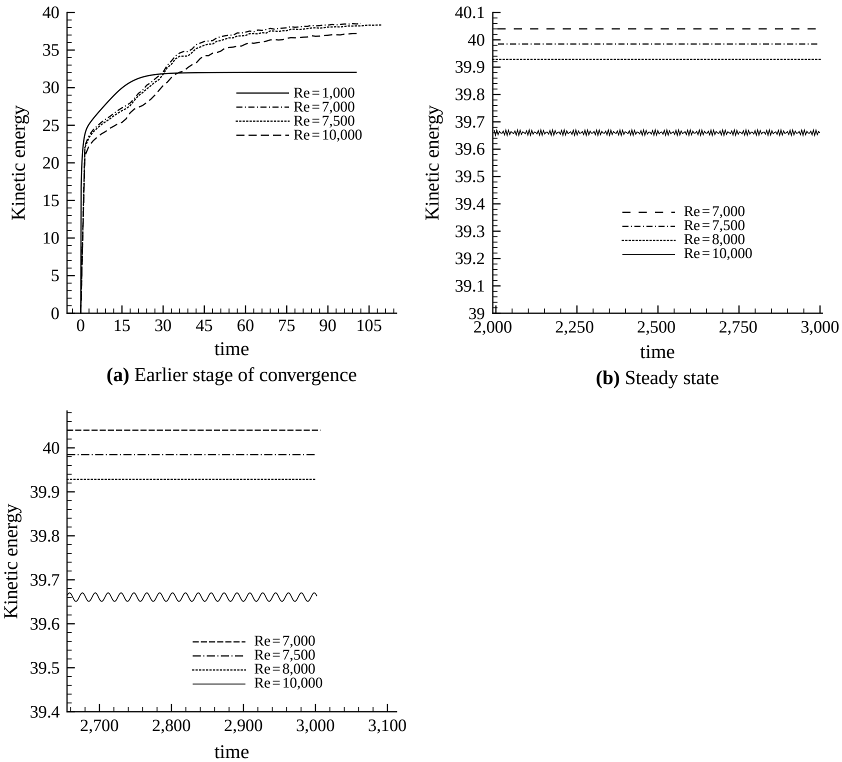

(a) Earlier stage of convergence

(b) Steady state

(c) Steady state: Close look at asymptotic state

Figure 10.
Kinetic energy convergence history

time $t = 30$. It means that the kinetic energy becomes a constant, i.e. the solution has reached a steady-state condition. Figure 10(b) shows the kinetic energy at steady state. At large time level, the kinetic energy for $Re < 8{,}000$ becomes a constant. However, at $Re = 10{,}000$, it is having an oscillating nature (Figure 10(c)). Authors feel that the TKE measure can also be a criterion for checking the attainment of steady-state.

Figure 11 shows the convergence history of TKE for uniform grids (257 × 257, $Re = 10{,}000$). The detailed time history are shown from Figure 12(a) to (j). The dimensionless periodic oscillation of TKE is observed with time. The period of oscillation calculated (measured from Figure 12(i) and (j)) for this case is 1.63. In other words, the frequency of oscillation is 0.61. The frequency of oscillation obtained by this method is exactly matching with the frequency $f = 0.61$ reported by Bruneau and Saad (2006). It is demonstrated that the present computation is able to capture the stable periodic solution after the bifurcation very accurately. Figure 13 shows the kinetic energy contour of the domain at $Re = 10{,}000$. The phase diagrams at bottom left, bottom right, top right and top left regions are shown in Figure 14(a)-(d). At the geometric center, an oscillation is observed (Figure 14(e)), though the magnitude is small compared to those at other locations. The streamline contours during a complete period are shown from Figure 15(a) to (k). It is observed that a tertiary vortex appears on the top left corner for $t = 0$ (reported by Barragy and Carey, 1997). It disappears at time $t = 0.96$. Complex behavior of secondary and tertiary vortices are also observed in bottom left and bottom tight corners. The left wall vorticity is shown during this period (Figure 16). It is having an oscillating nature.

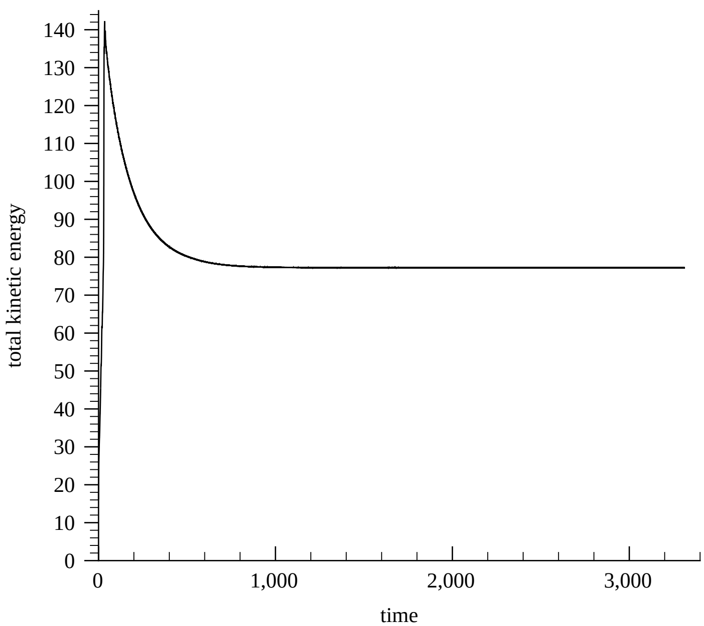

Figure 11.
Total kinetic energy convergence history: ($Re = 10{,}000$ (257 × 257))

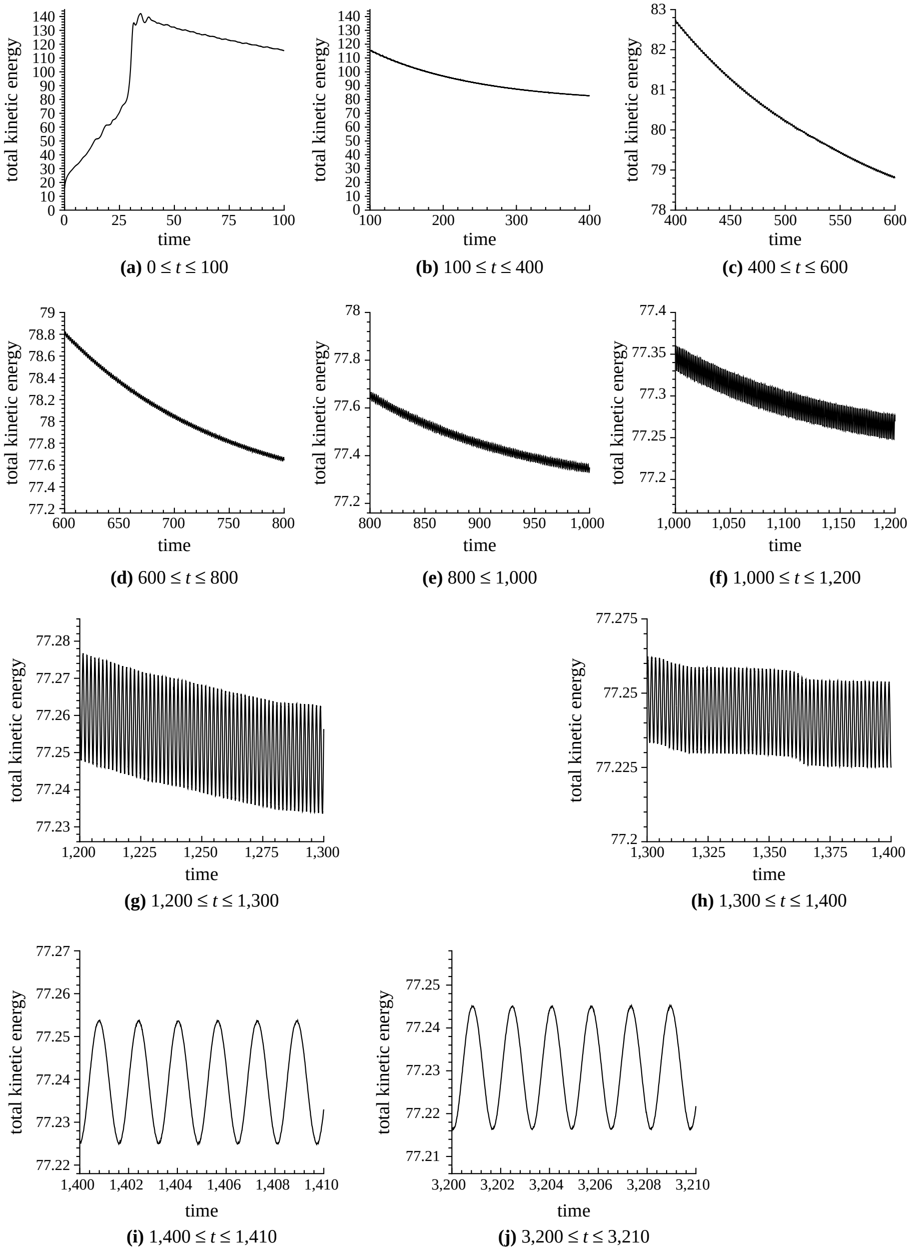

Figure 12.
Kinetic energy details

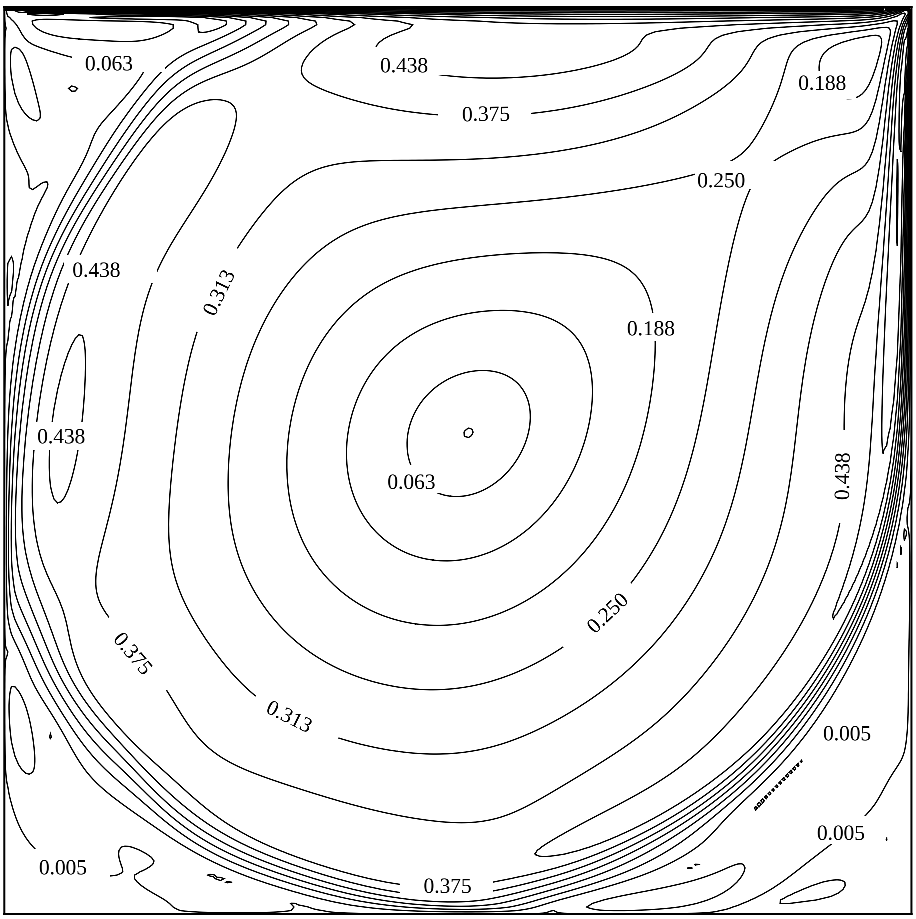

Figure 13.
Kinetic energy contour:
($Re = 10{,}000$ (257×257))

5. Conclusion

The square lid-driven cavity benchmark problem is solved by unsteady stream function-vorticity formulation using clustered grids. The discretization scheme is free from any upwinding scheme. The midplane velocity distribution and the top wall vortex distribution are compared with the results of other authors and found to be in good agreement with them. Transient study has demonstrated the time evolution of the eddy formation and the solution convergence. Kinetic energy variation with time is studied for large time computation. Below 7,500, it becomes a constant signifying the flow to be in steady-state. At $Re = 10{,}000$, the flow has an oscillating nature. The period of oscillation is found to be 1.63. It is demonstrated that the present computation is able to capture the stable periodic solution after the bifurcation very accurately. Authors feel that the kinetic energy can be a better measure for identifying the attainment of steady-state. The present clustered

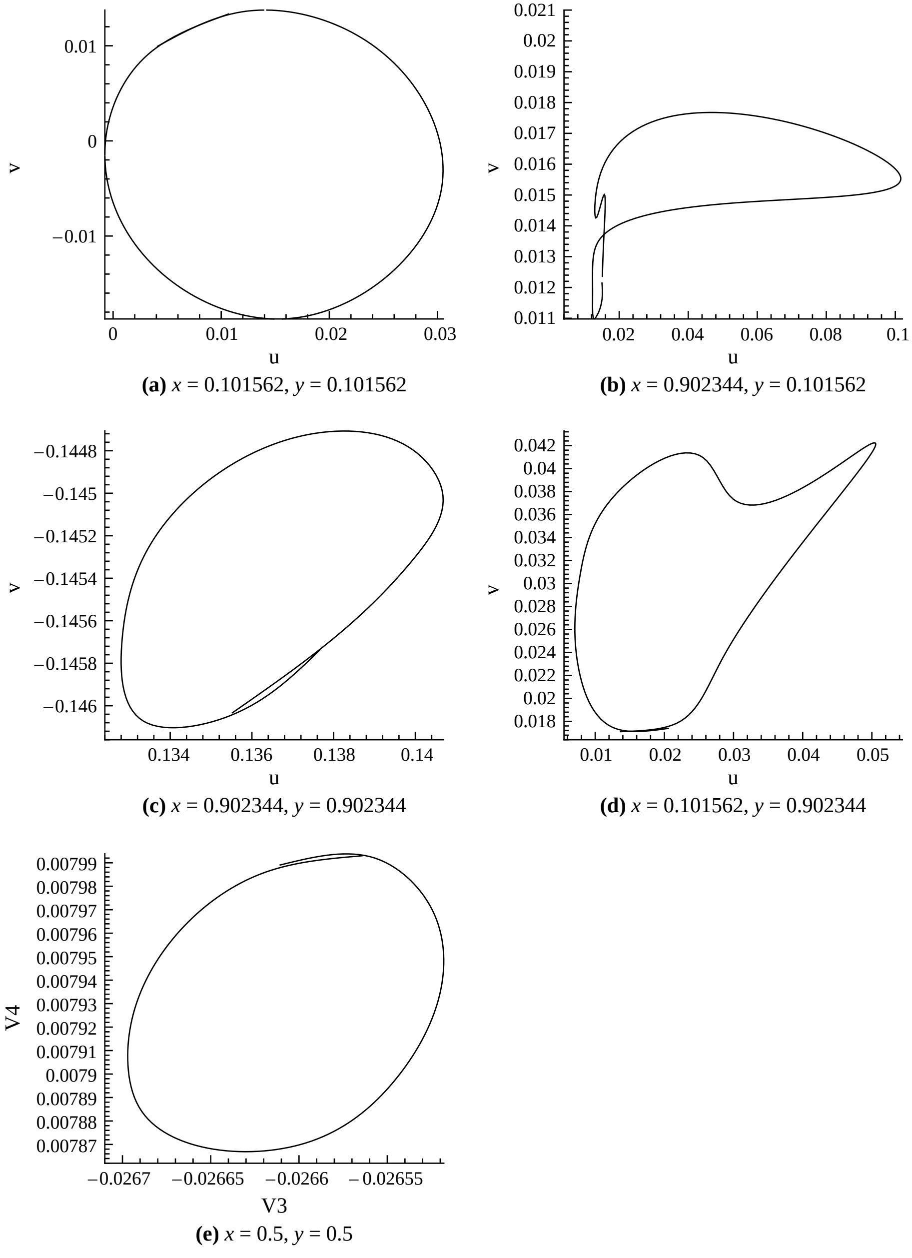

Figure 14.
Phase diagrams for uniform grid: $Re = 10{,}000$, 257×257

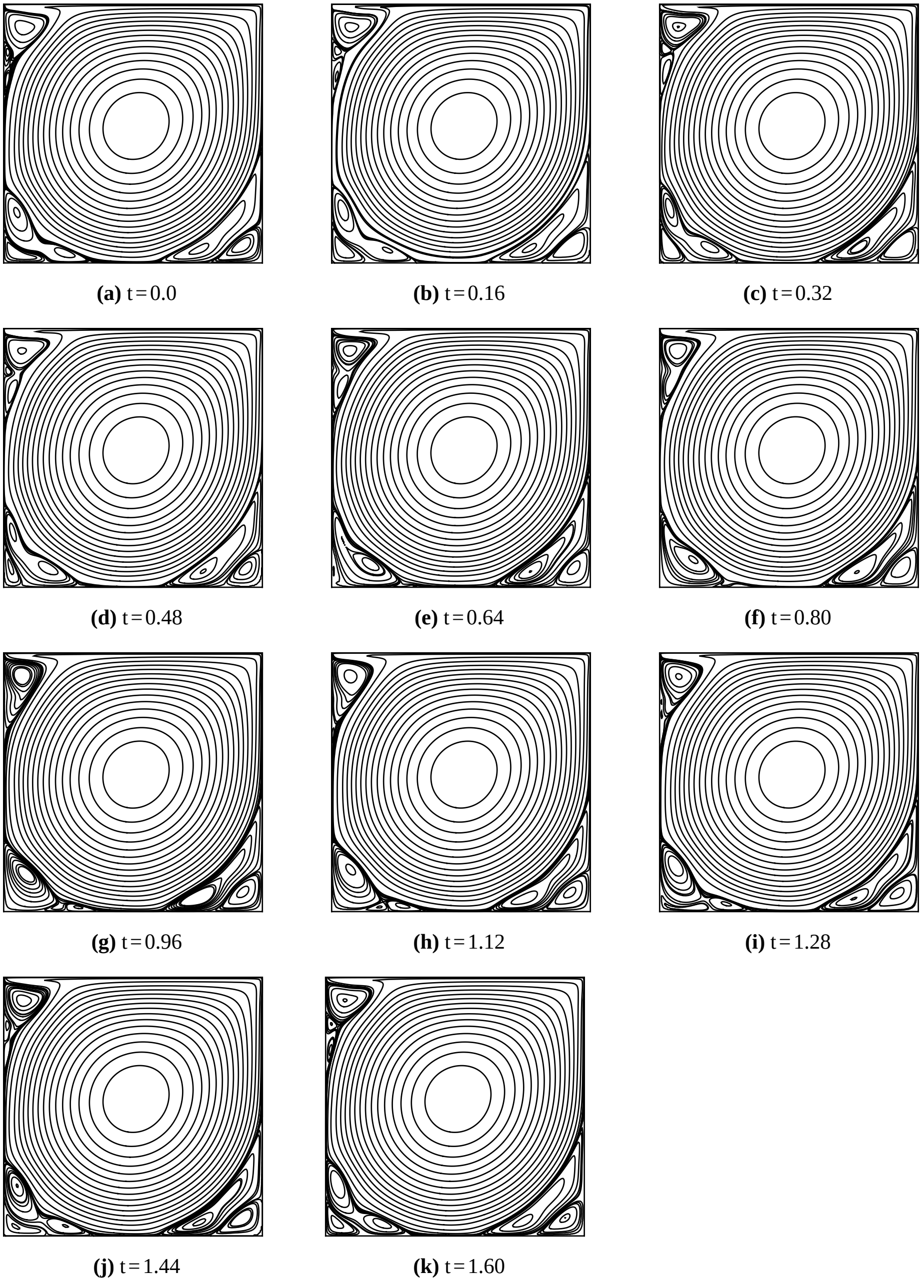

Figure 15.
Streamline contour during oscillation period: $Re = 10{,}000$, 257×257

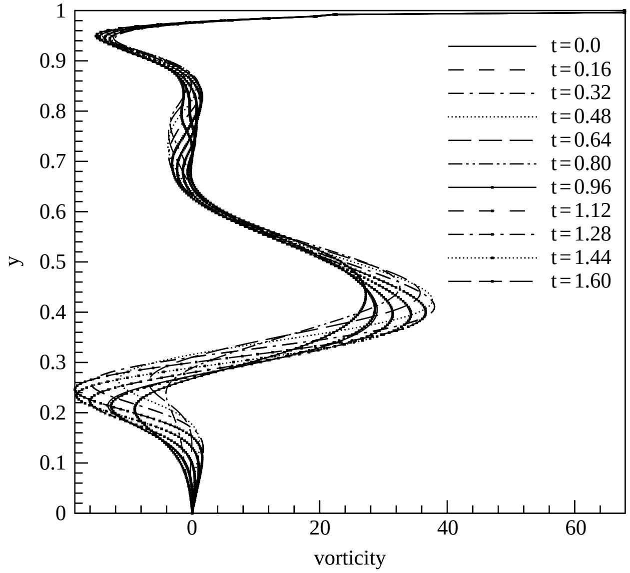

Figure 16.
Left wall vorticity: ($Re = 10{,}000$ (257×257))

grids computation has captured well the flow physics in the main recirculation and secondary recirculation zones.

References

Barragy, E. and Carey, G. (1997), "Stream function-vorticity driven cavity solution using *p* finite elements", *Computers & Fluids*, Vol. 26 No. 5, pp. 453-68.

Benjamin, A. and Denny, V. (1979), "On the convergence of numerical solutions for 2-D flows in a cavity at large Re", *Journal of Computational Physics*, Vol. 33, pp. 340-58.

Briley, W. (1971), "A numerical study of laminar separation bubbles using the Navier-Stokes equations", *Journal of Fluid Mechanics*, Vol. 47, pp. 713-36, part 4.

Bruneau, C-H. and Jouron, C. (1990), "An efficient scheme for solving steady incompressible Navier-Stokes equations", *Journal of Computational Physics*, Vol. 89, pp. 389-413.

Bruneau, C-H. and Saad, M. (2006), "The 2D lid-driven cavity problem revisited", *Computers & Fluids*, Vol. 35, pp. 326-48.

Burggraf, O. (1966), "Analytical and numerical studies of the structure of steady separated flows", *Journal of Fluid Mechanics*, Vol. 24, pp. 113-51.

Comini, G., Manzan, M. and Nonino, C. (1994), "Finite element solution of the stream function – vorticity equations for incompressible two-dimensional flows", *International Journal for Numerical Methods in Fluids*, Vol. 19, pp. 513-25.

Cortes, A. and Miller, J. (1994), "Numerical experiments with the lid driven cavity flow problem", *Computers & Fluids*, Vol. 23, pp. 1005-27.

Erturk, E., Corke, T. and Gokcol, C. (2005), "Numerical solutions of 2-D steady incompressible driven cavity flow at high Reynolds numbers", *International Journal for Numerical Methods in Fluids*, Vol. 48, pp. 747-74.

Ghia, U., Ghia, K. and Shin, C. (1982), "High resolutions for incompressible flow using the Navier-Stokes equations and multigrid method", *Journal of Computational Physics*, Vol. 48, pp. 387-411.

Goodrich, J., Gustafson, K. and Halasi, K. (1990), "Hopf bifurcation in driven cavity", *Journal of Computational Physics*, Vol. 90, pp. 219-61.

Goyon, O. (1996), "High-Reynolds number solutions of Navier-Stokes equations using incremental unknowns", *Computer Methods in Applied Mechanics and Engineering*, Vol. 130, pp. 319-35.

Gustafson, K. and Halasi, K. (1986), "Vortex dynamics of cavity flows", *Journal of Computational Physics*, Vol. 64, pp. 279-319.

Hou, S., Zou, Q., Chen, S., Doolen, G. and Cogley, A. (1995), "Simulation of cavity flow by the lattice Boltzmann method", *Journal of Computational Physics*, Vol. 118, pp. 329-47.

Huang, H. and Wetton, B. (1996), "Discrete compatibility in finite difference methods for viscous incompressible fluid flow", *Journal of Computational Physics*, Vol. 126, pp. 468-78.

Huser, A. and Biringen, S. (1992), "Calculation of two-dimensional shear-driven cavity flows at high Reynolds numbers", *International Journal for Numerical Methods in Fluids*, Vol. 14, pp. 1087-109.

Kim, J. and Moin, P. (1985), "Application of a fractional-step method to incompressible Navier-Stokes equations", *Journal of Computational Physics*, Vol. 59, pp. 308-23.

Kuyper, R., Meer, T.V.D., Hoogendoorn, C. and Henkes, R. (1993), "Numerical study of laminar and turbulent natural convection in an inclined square cavity", *International Journal of Heat and Mass Transfer*, Vol. 36 No. 11, pp. 2899-911.

Liao, S-J. and Zhu, J-M. (1991), "A short note on high-order streamfunction-vorticity formulations of 2D steady state Navier-Stokes equations", *Journal of Computational Physics*, Vol. 95, pp. 228-45.

Nallasamy, M. and Prasad, K. (1977), "On cavity flow at high Reynolds numbers", *Journal of Fluid Mechanics*, Vol. 79 No. 2, pp. 391-414.

Napolitano, M., Pascazio, G. and Quartapelle, L. (1999), "A review of vorticity conditions in the numerical solution of the ζ-ψ equations", *Computers & Fluids*, Vol. 28, pp. 139-85.

Peng, Y-F. and Shiau, Y-H. (1991), "Hopf bifurcation of the unsteady regularized driven cavity flow", *Journal of Computational Physics*, Vol. 95, pp. 228-45.

Poliashenko, M. and Aidun, C. (1995), "A direct method for computation of simple bifurcations", *Journal of Computational Physics*, Vol. 121, pp. 246-60.

Rek, Z. and Skerget, L. (1994), "Boundary element method for steady 2D high Reynolds-number flow", *International Journal for Numerical Methods in Fluids*, Vol. 19, pp. 343-61.

Roache, P. (1998), *Fundamentals of Computational Fluid Dynamics*, Chapter 3, Hermosa, Albuquerque, NM.

Schreiber, R. and Keller, H. (1983a), "Driven cavity flows by efficient numerical techniques", *Journal of Computational Physics*, Vol. 49, pp. 310-33.

Schreiber, R. and Keller, H. (1983b), "Spurious solutions in driven cavity calculations", *Journal of Computational Physics*, Vol. 49, pp. 165-72.

Shen, J. (1990), "Numerical simulation of the regularized driven cavity flows at high Reynolds numbers", *Computer Methods in Applied Mechanics and Engineering*, Vol. 80, pp. 273-80.

Shen, J. (1991), "Hopf bifurcation of the unsteady regularized driven cavity flow", *Journal of Computational Physics*, Vol. 95, pp. 228-45.

Sohn, J. (1988), "Evaluation of FIDAP on some classical laminar and turbulent benchmarks", *International Journal for Numerical Methods in Fluids*, Vol. 11, pp. 1469-90.

Tecplot 9.0-0.9 (2001), Amtec Engineering, Bellevue, WA.

Corresponding author
Manab Kumar Das can be contacted at: manab@iitg.ernet.in